CrystEngComm

PAPER

View Article Online
View Journal | View Issue

Cite this: *CrystEngComm*, 2014, **16**, 8726

Cu^{II}–PDC-bpe frameworks (PDC = 2,5-pyridinedicarboxylate, bpe = 1,2-di(4-pyridyl)ethylene): mapping of herringbone-type structures†

Francisco Llano-Tomé,[a] Begoña Bazán,*[ab] Miren-Karmele Urtiaga,[a] Gotzone Barandika,[c] Luis Lezama[bd] and María-Isabel Arriortua[ab]

Received 12th May 2014,
Accepted 18th July 2014

DOI: 10.1039/c4ce00989d

www.rsc.org/crystengcomm

Solid coordination frameworks (SCF) are crystalline materials based on connections between metal ions through organic ligands. In this sense, combination of polycarboxylate anions and dipyridyl ligands is an effective strategy to produce extended structures. In this context, this work is focused on two novel Cu^{II}-based SCFs incorporating PDC (2,5-pyridinedicarboxylate) and bpe (1,2-di(4-pyridyl)ethylene): $Cu_2[(PDC)_2(bpe)(H_2O)_2]\cdot 3H_2O\cdot DMF$ (**1**), and $Cu[(PDC)(bpe)_{0.5}(H_2O)]\cdot 2H_2O$ (**2**), where DMF is dimethylformamide. Both compounds were synthesized by slow evaporation, and their crystal structures were determined by X-ray diffraction. Further structural, thermal and magnetic characterization was carried out by means of IR, TG/DTG, DTA analysis, EPR, and measurements of the magnetic susceptibility. The crystallographic analysis revealed that compounds **1** and **2** can be described as herringbone-type layers formed by helicoidal Cu–PDC–Cu chains connected through bpe ligands. Solvent molecules are crystallized between the layers, providing the inter-layer connections through hydrogen bonds. Differences between the two compounds are attributable to these solvent molecules, being indicative of the flexibility of this type of SCFs. On the other hand, due to the variety of structures found in the literature that have been described as "herringbone arrays", this work also presents a crystallochemical study based on them. The study considers stoichiometry and structural parameters leading to the identification of two types of herringbone arrays, depending on the number of connections for the metal nodes (*i.e.* 3- and 4-connected).

Introduction

Solid coordination frameworks (SCF), also known as metal–organic frameworks (MOFs), have evolved over the last decade thanks to the variety of molecular complexes that can be formed using a broad range of organic ligands and metal ions.[1–4]

Their structural features, including large cavities and high surface areas, have opened up a wide range of applications[5] in fields such as gas storage,[6–8] gas separation,[9,10] heterogeneous catalysis,[11–14] drug delivery,[15–17] chemical sensing,[18–20] nonlinear optics[21,22] and biomedical imaging.[23]

One of the interesting points about these materials is the flexibility of the crystalline structures to allow the exchange of different solvents in host–guest chemistry.[24] The structural versatility of these molecular scaffolds is based on the large number of available ligands to create infinite topologies, with polycarboxylate spacers being some of the most used ligands. Among them, 2,5-pyridinedicarboxylate (PDC) is mentionable as it is a non-centrosymmetric ligand, exhibiting five potential donor atoms. In fact, this ligand has been observed to produce up to twenty-three coordination modes, and we first reported four of them as part of our research on the PDC ligand.[25–28] In this sense, we have been focusing our work on combinations of PDC with dipyridyl ligands. Thus, the work presented herein is devoted to the PDC-bpe combination (bpe = 1,2-di(4-pyridyl)ethylene). As shown in Scheme 1, where the Lewis structure for both ligands has been drawn, bpe can be found as two geometric isomers, *anti* and *gauche*, with the *anti* isomer being the most habitual.

The PDC-bpe combination has been poorly explored in the literature, as concluded from the fact that just two isostructural compounds (with Co^{II} and Zn^{II}) have been reported so far exhibiting this combination.[29] Thus, this work reports two novel Cu^{II}-based compounds with PDC

[a] *Departamento de Mineralogía y Petrología, Facultad de Ciencia y Tecnología, Universidad del País Vasco (UPV/EHU), Apdo 644, 48080 Bilbao, Spain. E-mail: bego.bazan@ehu.es; Fax: +34 946013500; Tel: +34 946012609*
[b] *BCMaterials Parque Tecnológico de Zamudio, Ibaizabal Bidea, Edificio 500-Planta 1, 48160, Derio, Spain*
[c] *Departamento de Química Inorgánica, Facultad de Farmacia, Universidad del País Vasco (UPV/EHU), Paseo de la Universidad, 7, 01006 Vitoria-Gasteiz, Spain*
[d] *Departamento de Química Inorgánica, Facultad de Ciencia y Tecnología, Universidad del País Vasco (UPV/EHU), Apdo 644, 48080 Bilbao, Spain*

† Electronic supplementary information (ESI) available: Crystallographic data, IR, TGA, distortion modes diagram. CCDC 997147 and 997148. For ESI and crystallographic data in CIF or other electronic format see DOI: 10.1039/c4ce00989d

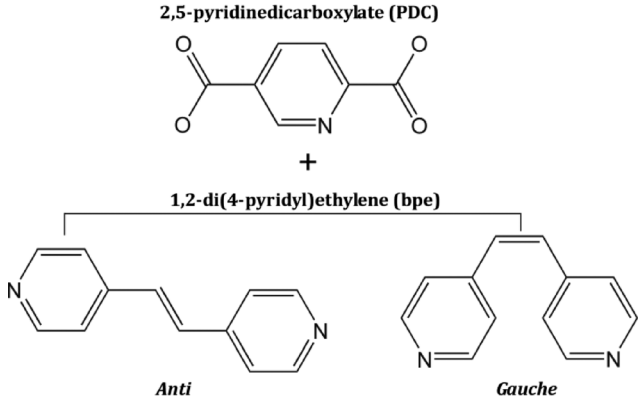

Scheme 1 Lewis structure for PDC and bpe ligands.

and bpe: $Cu_2[(PDC)_2(bpe)(H_2O)_2]\cdot 3H_2O\cdot DMF$ (**1**), and $Cu[(PDC)(bpe)_{0.5}(H_2O)]\cdot 2H_2O$ (**2**), where DMF is dimethylformamide. Both compounds were synthesized by slow evaporation, and their crystal structures were determined by X-ray diffraction. Further structural, thermal and magnetic characterization was carried out by means of IR, TG/DTG, DTA analysis, EPR, and measurements of the magnetic susceptibility. The crystallographic analysis revealed that compounds **1** and **2** can be described as herringbone-type layers.

The term "herringbone" is used in the literature to describe a variety of 2D arrays with four-connected nodes (4-c)[30–33] and three-connected nodes (3-c).[34–42] Scheme 2 shows that both arrays consist of the 2D packing of four-vertex polygons that exhibit nodes with three (3-c) and four connections (4-c), respectively.

As far as we are concerned, no distinction between these two possibilities has been made so far when describing 2D arrays as herringbone layers. Therefore, this work also presents a crystallochemical study stating the differences.

Additionally, as compounds **1** and **2** can be described as 3-c herringbone arrays, the study has been extended to other possible 3-c planar arrays. The conclusions lead to the identification of the structural features defining the 3-c herringbone arrays. Finally, several 3-c herringbone arrays found in the literature have been mapped (including compounds **1** and **2**). This mapping reveals the most favored structural features for this type of compound.

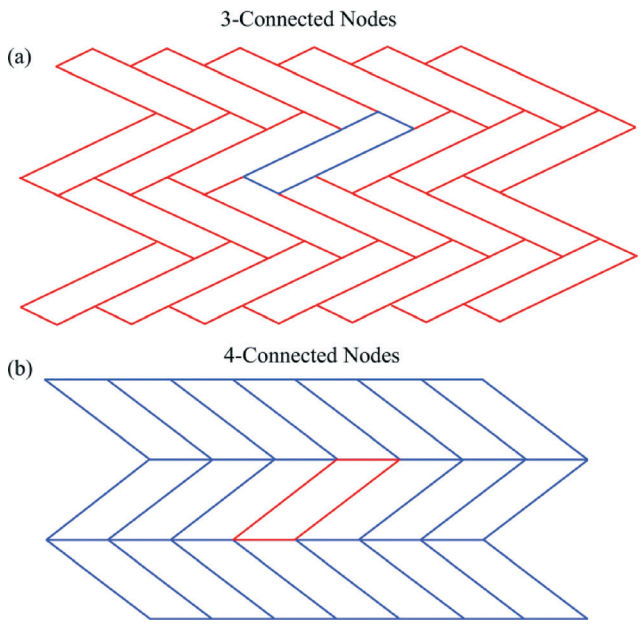

Scheme 2 2D herringbone arrays based on four-vertex polygons. Nodes can be (a) three-connected or (b) four-connected (4-c).

Experimental section

General

All solvents and chemicals were used as received from reliable commercial sources. The reactants 2,5-pyridinedicarboxylic acid (H_2PDC), 1,2-di(4-pyridyl)ethene (bpe), copper(II) nitrate hexahydrate 99%, triethylamine (Et_3N), and the solvent *N*,*N*-dimethylformamide (DMF) 99.8% were purchased from Sigma-Aldrich Co. Nitric acid 65% (HNO_3) was purchased from Panreac.

Synthesis of compound 1

H_2PDC (40.4 mg, 0.25 mmol), bpe (46.3 mg, 0.25 mmol) and $Cu(NO_3)_2\cdot 6H_2O$ (93.3 mg, 0.5 mmol) were dissolved in a solvent mixture of DMF–H_2O (10/10 mL) by stirring for 1 h at RT. The pH value was adjusted to 4.5 using Et_3N and HNO_3 (0.5 M). The resulting solution was sealed in a Teflon-lined autoclave for microwaves (XP1500), heating at 140 °C for 45 min in order to improve the solubility of the reagents. Then, the solution was filtered and poured into a glass crystallizing dish. After twelve hours, blue prismatic crystals were obtained. The sample was washed and dried with ethanol, and a crystal was collected for X-ray diffraction. The density was measured by the flotation method in a mixture of bromoform–choloroform, and was found to be 1.68(5) g cm^{-3} (found: C, 42.5(2); H, 3.59(2); N, 8.64(3). Calc. for $C_{29}H_{33}Cu_2N_5O_{14}$: C, 43.57; H, 3.75; N, 8.75. IR: ν_{max}/cm^{-1} 3415 (OH), 1656 and 1608 (aroC–C), 1286 (C–N), 1561 (asCOO), 1428, 1387 and 1352 (sCOO), 833, 770 and 692 (C–H) and 550–534 (Cu–N) (Fig. S1, ESI†)).

Synthesis of compound 2

H_2PDC (122.1 mg, 0.75 mmol), bpe (176.4 mg, 1 mmol) and $Cu(NO_3)_2\cdot 6H_2O$ (187 mg, 1 mmol) were dissolved in a solvent mixture of H_2O–MeOH (20/10 mL) by stirring for 30 min at RT. The pH value was adjusted to 4.5 using HNO_3 (0.5 M). The resulting solution was sealed in a Teflon-lined autoclave and heated at 120 °C for 72 h. The solution was slowly cooled to RT and filtered, pouring into a glass crystallized dish. After one day, light-green prismatic crystals were obtained. The sample was washed and dried with ethanol allowing the collection of one single-crystal for X-ray diffraction. The density was measured by the flotation method in a mixture of bromoform–chloroform, and was found to be 1.61(5) g cm^{-3}

(found: C, 41.87(2); H, 3.65(2); N, 7.50(3). Calc. for $C_{13}H_{10}CuN_2O_7$: C, 42.57; H, 3.54; N, 7.63. IR: ν_{max}/cm^{-1} 3410 (OH), 1656 and 1617 (aroC–C), 1281 (C–N), 1569–1560 (asCOO), 1428, 1390 and 1348 (sCOO), 834, 765 and 687 (C–H) and 551–534 (Cu–N) (Fig. S2, ESI†)).

Single-crystal X-ray diffraction

Prismatic single-crystals of compounds **1** and **2** with dimensions given in Table 1 were selected under a polarizing microscope and mounted on MicroMounts. Single-crystal data were collected at 100 K on an Agilent Technologies Supernova single source diffractometer with Cu-Kα radiation (1.54184 Å) for compounds **1** and **2**. Details of crystal data and some features of the structure refinements are reported in Table 1, and selected bond lengths and angles are listed in Tables S1 and S2 (ESI†).

Lattice constants were obtained by using a standard program belonging to the diffractometer software, confirming at the same time the good quality of the single-crystals. The Lorentz polarization and absorption corrections were made with the diffractometer software, taking into account the size and shape of the crystals.[43] The structures were solved by direct methods using the SIR92 (ref. 44) program, with the monoclinic *Pn* space group for compound **1**, and the $P2_1/n$ space group for compound **2**, which allowed us to obtain the positions of the copper atoms, as well as the oxygen and nitrogen atoms and some of the carbon atoms of both the PDC and bpe ligands of compounds **1** and **2**. The refinement of the crystal structures was performed by full-matrix least-squares based on F^2, using the SHELXL-97 (ref. 45) program, obtaining the remaining carbon atoms and allowing the allocation of the hydrogen atoms. Anisotropic thermal parameters were used for all non-hydrogen atoms (Fig. S3 and S4, ESI†). The hydrogen atoms belonging to the organic molecules were fixed geometrically and allowed to ride on their parent carbon atoms (C–H 0.93 Å), and were refined with common isotropic displacements. The positions of the hydrogen atoms bonded to the coordinating water molecules of compounds **1** and **2**, as well as the hydrogen atoms bonded to the crystallization water molecules of compound **1**, were fixed using DFIX and DANG instructions in the refinement to adjust the O–H distance to 0.82 Å and the H–O–H angle to 112°, respectively. All the crystallization water molecules for compound **2** were disordered in two groups. The hydrogen atoms of these water molecules were not considered due to the lack of density in the residual density map. One important point is that the DMF molecules break the $P2_1/n$ symmetry for compound **1**, resulting in the impossibility of locating the molecules of water and DMF in the cavities during refinement. Table S3† shows the crystallographic data corresponding to this structural resolution. This resolution permits the localization of the atoms corresponding to the layers. However, crystallization molecules of DMF and water cannot be localized. Therefore, the structure was solved in the *Pn* space group.

Physicochemical characterization techniques

The thermogravimetric analysis (TGA) was performed under air on a SDT 2960 Simultaneous DSC-TGA TA Instrument. The IR spectra were obtained with a Jasco FT/IR-6100 spectrophotometer in the 400–4000 cm^{-1} range with pressed KBr pellets. C, H and N elemental analyses were measured using a Euro EA 3000 Elemental analyzer.

Table 1 Details of the crystal data, structural resolution and refinement procedure for **1** and **2**

Compound	**1**	**2**
Formula	$C_{29}H_{33}N_5O_{14}Cu_2$	$C_{13}H_{10}N_2O_7Cu$
FW, g mol^{-1}	802.68	369.77
Crystal system	Monoclinic	Monoclinic
S. G., (no.)	*Pn*, (7)	$P2_1/n$, (15)
a, Å	11.4682(2)	11.3256(3)
b, Å	8.8977(1)	8.9352(2)
c, Å	15.6872(2)	15.1672(4)
β, °	94.074(1)	93.037(3)
V, $Å^3$	1596.69(1)	1532.71(3)
Z, *F*(000)	2824	4748
ρ_{obs}, ρ_{cal}, g cm^{-3}	1.68(5), 1.67	1.61(5), 1.60
μ, mm^{-1}	2.341	2.380
Crystal size, mm	0.096 × 0.064 × 0.035	0.108 × 0.072 × 0.03
Radiation, *λ*, Å	1.54184	1.54184
Temperature, K	100(10)	100(10)
Reflections collected, unique	11 540, 4648 (R_{int} = 0.027)	11 849, 3051 (R_{int} = 0.029)
Limiting indices	$-14 \leqq h \leqq 12$ $-10 \leqq k \leqq 11$ $-17 \leqq l \leqq 19$	$-14 \leqq h \leqq 14$ $-6 \leqq k \leqq 10$ $-18 \leqq l \leqq 18$
Final *R* indices [$I > 2\sigma(I)$]	R_1 = 0.029, wR_2 = 0.076	R_1 = 0.048, wR_2 = 0.137
R indices (all data)	R_1 = 0.031, wR_2 = 0.078	R_1 = 0.054, wR_2 = 0.144
Goodness of fit on F^2	1.041	1.014
Parameters/restraints	519/14	232/3
L. diff. peak and hole (e $Å^{-3}$)	0.776, −0.355	0.911, −0.534

Variable temperature (5–300 K) magnetic susceptibility measurements on polycrystalline samples were carried out with a Quantum Design MPMS-7 SQUID magnetometer under a magnetic field of 0.1 T. The experimental susceptibilities were corrected for the diamagnetism of the constituent atoms by using Pascal's tables. X-band EPR measurements were carried out on a Bruker ELEXSYS 500 spectrometer with a maximum available microwave power of 200 mW and equipped with a super-high-Q resonator ER-4123-SHQ and standard Oxford low temperature devices. For Q-band studies, EPR spectra were recorded on a Bruker EMX system equipped with an ER-510-QT. The magnetic field was calibrated by a NMR probe and the frequency inside the cavity was determined with a Hewlett-Packard 5352B microwave frequency counter. Computer simulation: WINEPR-Simfonia, version 1.5, Bruker Analytische Messtechnik GmbH.

Results and discussion

Crystal structures

The crystal structures for compounds $Cu_2[(PDC)_2(bpe)(H_2O)_2]\cdot 3H_2O\cdot DMF$ (**1**) and $Cu[(PDC)(bpe)_{0.5}(H_2O)]\cdot 2H_2O$ (**2**) are quite similar, so they will be described together. In fact, both compounds consist of 2D arrays of the so-called herringbone type. These layers are interconnected *via* hydrogen bonds through the crystallization molecules (1 DMF and 3 water molecules per 2 Cu^{II} ions in compound **1**, and 4 water molecules per 2 Cu^{II} ions in compound **2**), giving rise to a 3D supramolecular framework (Fig. 1), with channels along the [010] direction (Tables S4 and S5, ESI†).

The 2D arrays are formed by zig-zag chains of Cu–PDC–Cu. This is reflected in the helical axis for compound **2** (space group $P2_1/n$) but, as explained above, the presence of DMF in compound **1** leads to a lower symmetry of the framework (space group Pn). These chains are interconnected through the bpe ligands, producing the herringbone pattern (Fig. 2).

The torsion angles of the bpe ligand for compounds **1** and **2** are 7.15° and 1.47°, respectively. Therefore, bpe exists in these compounds as the *anti* geometric isomer.

The asymmetric unit for compound **1** is formed by two crystallographically independent Cu atoms (Cu1 and Cu2). This way, the Cu1···Cu2 and Cu2···Cu1^{i} (i = x, $-1+y$, z) distances in the chain for compound **1** are 7.271(2) Å and 7.235(2) Å, respectively. The Cu1–Cu2–Cu1^{i} and Cu2^{ii}–Cu1–Cu2 (ii = x, $1+y$, z) angles are the same, being 75.67°(1) in both cases. In the case of compound **2**, the Cu1···Cu1^{i} (i = $1/2-x$, $-1/2+y$, $3/2-z$) distance is 7.210(5) Å, and the Cu1^{ii}–Cu1–Cu1^{i} (ii = $1/2-x$, $1/2+y$, $3/2-z$) angle is 76.58°(5).

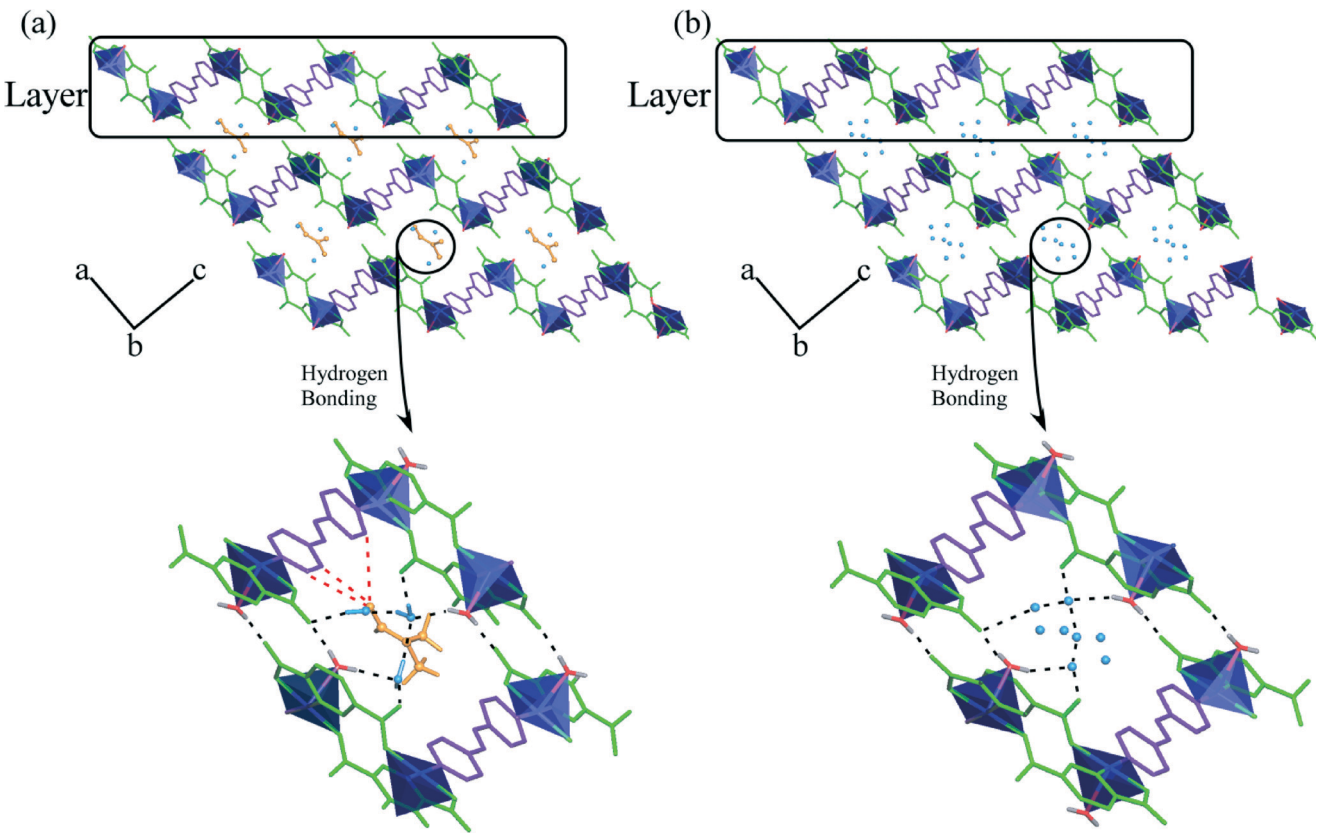

Fig. 1 3D supramolecular frameworks for compounds **1** (a) and **2** (b). The PDC and bpe ligands are colored in green and purple, respectively. (Bottom left) Zoomed image of the crystallization molecules of DMF (orange) and water (blue) for compound **1**, connected to the layers through hydrogen bonds (red and black) and water (blue), and (bottom right) zoomed image of the disordered crystallization molecules of water (blue) for compound **2** (all hydrogen atoms are omitted for clarity).

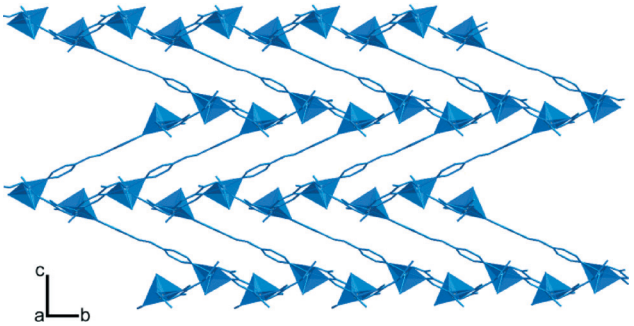

Fig. 2 2D herringbone layer observed for compound **1**.

For compound **1**, as well as for compound **2**, the Cu atoms have a square pyramidal coordination environment, being coordinated to two oxygen atoms and a nitrogen atom (from two different PDC ligands), to a nitrogen atom belonging to a bpe ligand in the equatorial plane, and to a water molecule in the apical position.

In both cases, the Cu–O distances lie within the range 1.934(2)–2.220(1) Å, and the Cu–N distances exhibit values between 2.010(3)–2.033(1) Å, as reported for other complexes containing Cu^{II} (Tables S1 and S2, ESI†). The most significant bond distances and angles are reported in Tables S6 and S7 (ESI†), respectively. In summary, the difference between the two compounds lies in the solvent molecules connecting the layers, which is indicative of the flexibility of this type of compound.

As noted previously, there are channels along the [010] direction, and their diameter has been evaluated by means of the Voronoi–Dirichlet polyhedra, which were constructed through the Dirichlet program included in TOPOS[46] (Fig. S5, ESI†). As observed, both compounds show a straight channel path. The diameters (D) are quite similar: D_{max} = 2.888 Å (for **1**) and 2.818 Å (for **2**), and D_{min} = 2.588 Å (for **1**) and 2.512 Å (for **2**). In fact, compound **1** exhibits the largest cavities, corresponding to the fact that DMF molecules are larger. As observed, the interlayer distance is consistent with the higher size of DMF (Fig. S6, ESI†).

Topological features for compounds **1** and **2** were analyzed by means of the TOPOS[46] software, revealing a hcb Shubnikov hexagonal plane net (point symbol = 6^3 and vertex symbol = [6.6.6]), corresponding to the topology shown in Scheme 2a. Further discussion on topology is given in the section devoted to the mapping of 3-c herringbone-arrays.

Distortion of coordination spheres for metal centres

Distortion of coordination polyhedra was evaluated according to the Avnir[47,48] method, based on the continuous symmetry measures (CSM), using the SHAPE[49] program, and the results can be seen in Table 2. The projection of the as-calculated values on the distortion diagram can be seen in Fig. S7 (ESI†). As observed for the three analyzed Cu^{II} ions, distortion occurs *via* a non-Berry pathway that converts the trigonal bypiramid into a square pyramid[50] (SPY) with a soft contribution of a vacant octahedron (VOC) distortion. In fact, for Cu1 and Cu2 in compound **1**, the axial distances (Cu1–O5 = 2.259(3) Å and Cu2–O6 = 2.216(3) Å) are longer than the equatorial ones (ranging from 1.947(3) Å to 2.030(3) Å). Similarly, for compound **2**, the axial distance Cu1–O1W is 2.245(3) Å and the equatorial distance ranges from 1.943(2) Å to 2.027(3) Å.

Table 2 Geometrical distortions of the trigonal bypiramid (TBPY) and Berry square pyramid (SPY), calculated using SHAPE software

Compound	Pentacoordinate	S (TBPY)	S (SPY)
1	Cu(1)	5.49	1.19
	Cu(2)	5.37	1.13
2	Cu(1)	5.70	1.13

Thermogravimetry

In order to study the thermal stability of compounds **1** and **2**, thermogravimetric (TG) analysis was performed.

Compound **1** shows two stages of mass loss (Fig. S8, ESI†). The first of them, starting at RT and finishing at about 165 °C, has been assigned to the removal of the crystallization and coordination molecules of water and DMF (20.3% calc. and 22.2% exp.). The second one (63.83% calc. and 62.74% exp.) is an abrupt mass loss, and corresponds to the removal of both organic ligands occurring between 255 °C and 345 °C. The residue has been identified by X-ray powder diffraction as CuO.[51]

The TG analysis of compound **2** shows a mass loss of 15.4% from RT to 86 °C (Fig. S9, ESI†), attributed to the crystallization and coordination molecules of water (14.44% calc.). The curve shows a plateau up to 280 °C, when the calcination of the organic molecules takes place with a mass loss of 64.24% (68.54% calc.). The calcination product was also CuO.[51]

Mapping of 3-c herringbone-arrays

As noted previously (Scheme 2), herringbone arrays are produced by the 2D packing of four-vertex polygons that can be three- (3-c) and four-connected (4-c). If those topologies are translated to an ideal array consisting of metal nodes and two organic ligands (A and B), the result is that four-vertex polygons are produced by four-metal nodes in a 4-c herringbone array but by six-metal nodes for a 3-c array (Scheme 3). Both types of layer differ in stoichiometry, being $M_1A_1B_1$ for 4-c planes, and M_2A_2B for 3-c ones. As observed in Scheme 3, both types of arrays have in common the zig-zag chain (green), which is extended by metal nodes sharing A ligands. The connections between these chains through B ligands (purple) is the distinguishing factor between the two arrays. In summary, $M_1A_1B_1$ stoichiometry in 4-c planes produces four-vertex/four-node polygons, while M_2A_2B for 3-c ones produces four-vertex/six-node polygons.

Since compounds **1** and **2** exhibit 3-c herringbone planes, the following discussion refers to 2D arrays based on 3-c nodes.

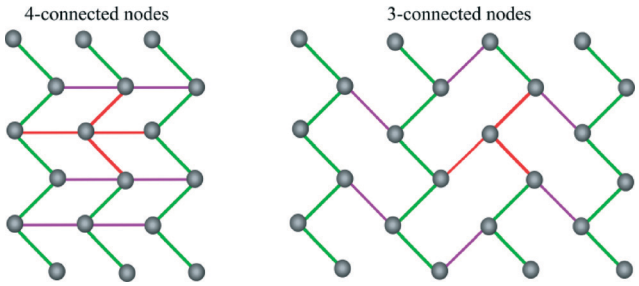

Scheme 3 (Left) 4-c and (right) 3-c herringbone 2D arrays. Green and purple lines represent A and B ligands, respectively. Lines in red mark the 4-c and 3-c nodes.

It is worth noting that in the ideal array shown in Scheme 3, all the nodes are coplanar. Additionally, distances between metal nodes through A (*d*A, green) and B (*d*B, purple) ligands are identical (*d*A = *d*B), producing a high-symmetry plane. Considering that an ideal geometry is highly symmetrical, the 3-c herringbone array shown in Scheme 3 is just one of the ideal possibilities for 3-c nodes to extend in planes so as to produce six-node polygons. In fact, as shown in Scheme 4, there are two other ideal geometries for *d*A/*d*B = 1. Therefore, there are three possibilities: the first is based on a brick-wall sheet; the second consists of regular hexagons; and the third is a 3-c herringbone array. The "a_1", "a_2" and "a_3" angles defined in Scheme 4 for the nodes mark the differences between these three possibilities.

As shown in Scheme 4, the transition from hexagon-based plane to brick-wall sheet and 3-c herringbone array causes the a_2 angle to change from 120° to 90° in both cases. Therefore, the $a_1 - a_3$ parameter becomes −90° for the brick-wall sheet and +90° for the 3-c herringbone array. It is also worth noting that the hexagonal array does not permit *d*A and *d*B to be different. However, the brick-wall sheet and 3-c herringbone array can be produced in cases where the distances are not equal (*d*A ≠ *d*B).

As mentioned previously, compounds **1** and **2** exhibit 3-c herringbone planes, but their "a_2", "$a_1 - a_3$" and "*d*A/*d*B" parameters are far from those corresponding to high symmetry. In fact, Scheme 5 represents the real situation for both compounds, where the non-coplanarity of the six nodes

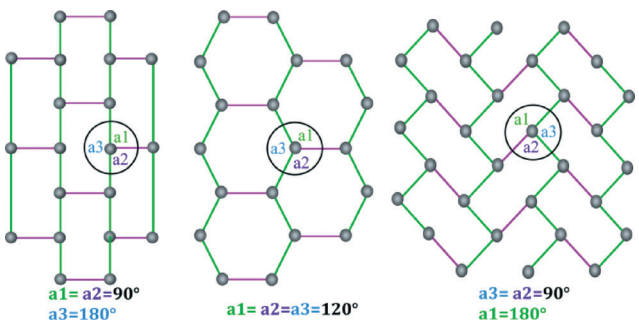

Scheme 4 Possibilities for high-symmetry planes based on 3-c nodes according to angles "a_1", "a_2", and "a_3". (Left) Brick-wall sheet, (center) regular hexagons, and (right) herringbone array.

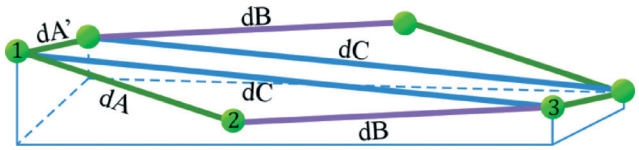

Scheme 5 Four-vertex/six-node polygons in real (non-coplanar) 3-c herringbone arrays.

can be observed. Thus, if we take three consecutive nodes (1, 2 and 3), the *d*C parameter (blue line) can be defined as the distance between nodes 1 and 3 (nodes 1 and 2 being linked through an A ligand, and nodes 2 and 3 being linked through a B ligand).

It is also worth noting that in real structures, two distances through the A ligand can be defined: *d*A and *d*A′. In most cases, both distances are quite similar. Thus, the four-vertex polygons are formed by *d*A′–*d*C–*d*A′–*d*C sides while the six-node ones are formed by *d*A–*d*B–*d*A′–*d*A–*d*B–*d*A′ sides. The situation is similar for other compounds found in the literature.[34–42] Finally, while in an ideal 3-c herringbone array the sum of *d*A and *d*B distances is *d*C due to the coplanarity of the six nodes (*d*A + *d*B = *d*C), in real compounds the sum of *d*A and *d*B distances is different to *d*C (*d*A + *d*B ≠ *d*C). Therefore, a *d*B* distance has also been defined (*d*B* = *d*C − *d*A).

Table 3 collects these angles and distances for several compounds found in the literature that are described as herringbone arrays.[34–42] The selection in Table 3 is not intended to be exhaustive, since more than 2300 compounds have been found in the TOPOS[46] database exhibiting the 3-c topology shown in Scheme 1.

However, many of these topologies refer to connections between M–A–M zig-zag chains through hydrogen bonds, and this is not the case under study in this work. On the other hand, there are singular characteristics in many of the so-called herringbone-arrays that do not fit with the description herein, such as the coordination number of the metal centers (4-c), angles M–A–M that do not lie within these herringbone arrays, and the dimensionality of the frameworks.

The purpose of our selection is for it to be representative of similar arrays to the one found for compounds **1** and **2**. For example, one of the discarded compounds is [Zn(H_2MBP)(IPA)]·H_2O, described by S. Sengupta *et al.*[37] as herringbone together with other Zn-H_2MBP compounds. The reason for discarding this compound in this study is that its parameters indicate that the 3-c array is close to ideal hexagonal but tending towards a brick-wall sheet as opposed to a 3-c herringbone array ($a_1 - a_3$ = −3.24°, *d*A/*d*B = 1.16, and *d*A/*d*B* = 1.17).

As noted previously, the 3-c herringbone array is consistent with M_2A_2B stoichiometry. Therefore, some explanations are required for the compounds in Table 3, in order to avoid confusion.

Firstly, in compound [Zn(4,4-bipyridine)(Hptc)H_2O]$_n$,[34] half of the Hptc ligands do not act as connectors, so the stoichiometry for the bridging ligands is in fact Zn(4,4-bipyridine)(Hptc)$_{0.5}$, as expected. Secondly, in

Table 3 Structural parameters for selected "herringbone" arrays

Compound	*d*A (Å)	*d*A′ (Å)	*d*B (Å)	*d*C (Å)	*d*B* (Å)	a_1 (°)	a_2 (°)	a_3 (°)	$a_1 + a_2 + a_3$
$[Cu(PDC)(bpe)_{0.5}(H_2O)]\cdot 2H_2O$	7.21	7.21	13.43	19.32	12.11	136.77	66.34	76.58	279.69
$[Cu_2(PDC)_2(bpe)(H_2O)_2]\cdot 3H_2O\cdot DMF$	7.27	7.23	13.44	19.42	12.15	137.19	68.07	75.67	280.93
[Zn(4,4-bipyridine)(Hptc)·H_2O][34]	5.34	5.34	11.06	15.67	10.33	143.20	76.98	84.03	304.21
[Cd(hmph)(dpa)]·H_2O[35,36]	5.62	12.06	11.88	12.58	6.97	148.27	79.77	82.07	310.11
$[Zn(H_2MBP)(Br\text{-}IPA)]_n\cdot CH_3OH$[37]	8.97	8.97	7.72	15.80	6.83	142.41	71.67	119.17	333.25
$[Zn(H_2MBP)(CH_3\text{-}IPA)]_n\cdot CH_3OH$[37]	9.02	9.02	7.76	15.74	6.71	139.10	74.97	121.01	335.08
$[Cu_2(3,5\text{-}(NO_2)_2sal)_2(4'4\text{-bipy})(H_2O)]_n$[38,39]	5.02	5.02	11.11	16.00	10.98	164.09	67.02	106.78	337.89
$[Pr(bib)_2(NO_3)_3]$[40]	14.73	14.73	15.27	29.84	15.11	168.26	70.84	102.90	342.00
$[Cd_2(azpy)_3(NO_3)_4]\cdot 2Me_2CO$[41]	13.44	13.44	13.66	26.67	13.23	159.52	81.38	102.68	343.58
$[Cd_2(NO_3)_4(4,4'\text{-azpy})_3]\cdot CH_2Cl_2\cdot xH_2O$[39,42]	13.15	13.15	13.31	26.00	12.85	158.62	82.54	102.90	344.06
$[Co_2(NO_3)_4(4,4'\text{-azpy})_3]\cdot CH_2Cl_2\cdot xH_2O$[42]	13.30	13.30	13.36	26.25	12.94	159.78	81.06	104.46	345.30
$Zn[(H_2MBP)(OME\text{-}IPA)]\cdot n(H_2O)$[37]	8.57	8.57	8.12	14.88	6.30	163.35	75.88	120.39	359.62

compounds with Zn and H_2MBP,[37] there are double bridges through Br-IPA, CH_3-IPA and OME-IPA ligands, so two ligands account for a single A unit.

Additionally, in compounds $[M_2(NO_3)_4(4,4'\text{-azpy})_3]\cdot CH_2Cl_2\cdot X(H_2O)$[39,42] (M = Cd, Co), the ligand 4,4′-azpy plays both roles (acting as A and B ligands); so there are three ligands for every two metal ions. Thirdly, in compound $[Pr(bib)_2(NO_3)_3]$,[40] the nitrate oxoanions do not act as connectors, and the bib ligand acts as both A and B, but establishes double bridges when acting as B.

Finally (and similarly), in compound $[Cd_2(azpy)_3(NO_3)_4]\cdot 2Me_2CO$,[41] the nitrate groups are terminal ligands, and the azpy connector plays the role of both A and B ligand (with single bridges for both).

All the compounds in Table 3 exhibit $a_1 + a_2 + a_3$ values distinct from the ideal value of 360°, which is consistent with the lack of coplanarity. Taking into account the relationship between a_1, a_2 and a_3 angles (Scheme 4), the a_2 parameter has been represented *vs.* the $a_1 - a_3$ parameter (Fig. 3).

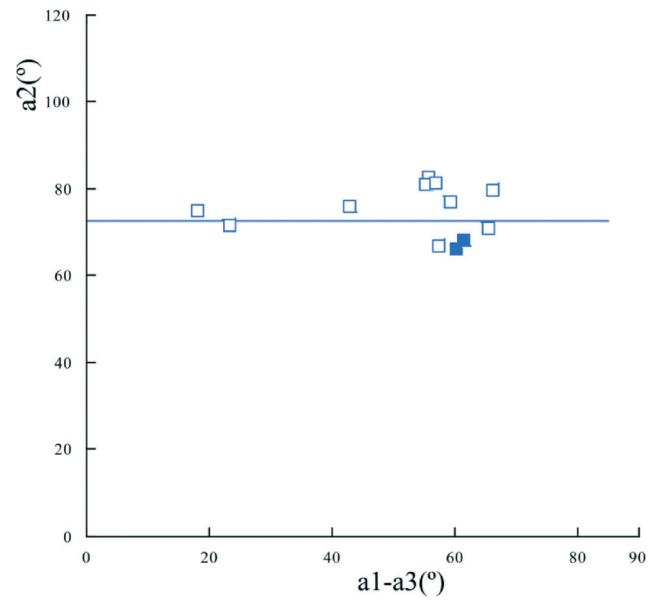

Fig. 3 Representation of the a_2 parameter *vs.* the $a_1 - a_3$ parameter for the compounds in Table 3. Compounds **1** and **2** are marked by filled symbols.

Most of the compounds are located on the same zone of the graph. It is also worth noting that dispersion for the a_2 values (that is, the zig-zag angle for the M–A–M chain) is very low (the average a_2 value is 74(5)°, while values of $a_1 - a_3$ range from 18.09° to 61.52°, and the majority are located around $a_1 - a_3 = 60°$).

In order to have an holistic view of the question (including the effect of distances), *d*A/*d*B and *d*A/*d*B* values have been represented *vs.* the $a_2/(a_1 - a_3)$ parameter (Fig. 4). It can be observed that the change of *d*A/*d*B and *d*A/*d*B* with the $a_2/(a_1 - a_3)$ parameter is similar. Thus, values of *d*A/*d*B decrease for decreasing values of $a_2/(a_1 - a_3)$, the slope becoming abrupt as $a_2/(a_1 - a_3)$ tends to 1 (the value for the ideal 3-c herringbone array).

The general trend observed in Fig. 4 should be corroborated with more structural data. Thus, our contribution is the identification of the structural parameters defining a 3-c herringbone array, and the proposal of a correlation between angles and distances in this type of structure.

Electronic paramagnetic resonance

X- and Q-band EPR measurements were carried out on powdered samples at several temperatures in the range 5–300 K.

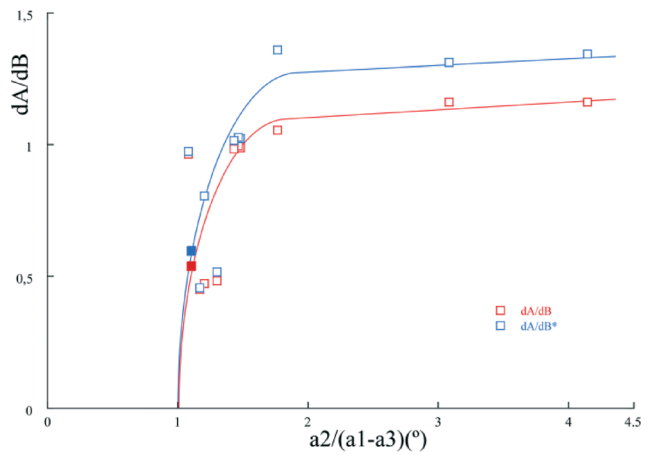

Fig. 4 Representation of *d*A/*d*B and *d*A/*d*B* values *vs.* the $a_2/(a_1 - a_3)$ parameter for compounds in Table 3. Compounds **1** and **2** are marked by filled symbols.

Due to the structural similarities in compounds **1** and **2**, compound **1** was selected for measurements, as it contains two crystallographically independent metal atoms. The X-band powder EPR spectrum of compound **1** shows the characteristic shape of Cu^{II} sites with axial symmetry, remaining practically unchanged from RT down to 5 K. However, for the Q-band measurement, a rhombic signal is observed (Fig. 5).

The spin Hamiltonian parameters were estimated by comparison of the experimental spectra with those obtained using a computer simulation program working at the second order of the perturbation theory. The parameters were optimized by the trial-and-error method and the best-fit results are represented as dashed lines in Fig. 5. The principal components of the *g*-tensor are $g_1 = 2.261$, $g_2 = 2.103$ and $g_3 = 2.062$ ($g_{iso} = 2.142$). The absence of hyperfine structure is indicative of the magnetic exchange between non-equivalent Cu^{II} ions.

Magnetic properties

The thermal variation of the inverse of the magnetic molar susceptibility (χ_m^{-1}) and the $\chi_m T$ product ($\mu_{eff}^2 = 8\chi_m T$) for compound **1** is shown in Fig. 6.

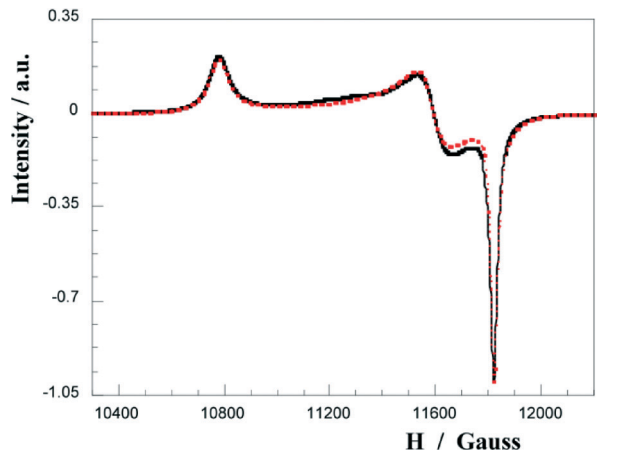

Fig. 5 Q-band EPR spectrum for compound **1**.

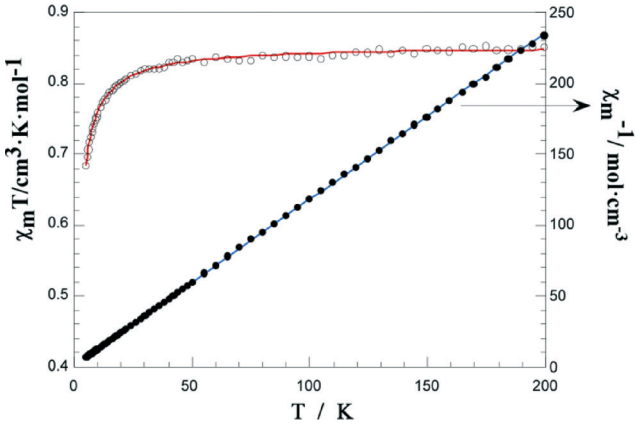

Fig. 6 Temperature dependence of $\chi_m T$ of compound **1**.

The effective magnetic moment exhibits a plateau from RT to 20 K having a value of 2.6 μB, and decreases to a value of 2.3 μB at 5 K. Above 10 K, the magnetic susceptibility follows the Curie–Weiss law with $C_m = 0.85$ cm^3 K mol^{-1} and $\theta = -1.4$ K. Both the negative temperature intercept and the decrease of the effective magnetic moment at low temperature are in agreement with weak antiferromagnetic interactions in the compound (in accordance with EPR analysis).

According to the structural features, the magnetic measurements on **1** have been fitted using Bonner and Fisher's expression (eqn (1)) for chains of equally spaced copper(II) ions, derived from the Heisenberg–van Vleck–Dirac Hamiltonian for isotropic magnetic 1D systems with spin $S = 1/2$ (eqn (2)).[52,53] The best least-square fitting was achieved for $J/k = -0.95$ K (0.66 cm^{-1}) and calculated $g = 2.13$ (experimental EPR value is 2.14).

$$X_m = \frac{Ng^2\beta^2}{KT}\frac{0.25 + 0.074975x + 0.075235x^2}{1 + 0.9931x + 0.172135x^2 + 0.757825x^3} \quad (1)$$

$$H = -2J\sum_{i=1}^{n-1} S_{Ai} \bullet S_{AiH} \quad (2)$$

where

$$x = \frac{|2J|}{KT}.$$

Conclusions

The combination of PDC and bpe ligands to produce SCFs (also known as MOFs) has been poorly explored thus far. In this context, we have prepared two 2D compounds using these ligands, and Cu^{II} as a metal node. Both compounds exhibit similar structural features consisting of herringbone arrays and solvent molecules located between layers. These crystallization molecules provide the hydrogen bonds that stabilize the 3D framework. The fact that similar 3D arrays are produced with different solvent molecules is indicative of the flexibility of this type of compound.

The use of the term "herringbone" in the literature is widespread and can lead to confusion, so we have identified two types of herringbone array (4-c and 3-c) depending on the number of connections for each metal node. In this sense, $M_1A_1B_1$ stoichiometry corresponds to 4-c arrays, while M_2A_2B stoichiometry corresponds to 3-c ones (M is the metal ion, and A and B are the organic ligands).

We have also identified the structural parameters defining the 3-c herringbone arrays (as adopted by the compounds reported in this work), and have observed a correlation between angles and distances in this type of structure. Finally, we have studied a set of compounds referred to as herringbone networks, and have found that the M–A–M chain zig-zag angle exhibits values close to 74° in all cases.

Acknowledgements

This work has been financially supported by the "Ministerio de Economía y Competitividad" (MAT2013-42092-R) and the "Gobierno Vasco" (Basque University System Research Group, IT-630-13), which we gratefully acknowledge. SGIker (UPV/EHU) technical support (MEC, GV/EJ, and European Social Fund) is gratefully acknowledged. F. Llano-Tomé thanks the "Ministerio de Ciencia e Innovación" for a fellowship (BES-2011-045781).

Notes and references

1 H. Furukawa, K. E. Cordova, M. O'Keeffe and O. M. Yaghi, *Science*, 2013, **341**, 974.
2 M. O'Keeffe and O. M. Yaghi, *Chem. Rev.*, 2012, **112**, 675–702.
3 M. Li, D. Li, M. O'Keeffe and O. M. Yaghi, *Chem. Rev.*, 2014, **114**, 1343–1370.
4 T. R. Cook, Y.-R. Zheng and P. J. Stang, *Chem. Rev.*, 2013, **113**, 734–777.
5 C. Wang, D. Liu and W. Lin, *J. Am. Chem. Soc.*, 2013, **135**, 13222–13234.
6 F. Gandara, H. Furukawa, S. Lee and O. M. Yaghi, *J. Am. Chem. Soc.*, 2014, **136**, 5271–5274.
7 D. J. Tranchemontagne, K. S. Park, H. Furukawa, J. Eckert, C. B. Knobler and O. M. Yaghi, *J. Phys. Chem. C*, 2012, **116**, 13143–13151.
8 T. A. Makal, J.-R. Li, W. Lu and H.-C. Zhou, *Chem. Soc. Rev.*, 2012, **41**, 7761–7779.
9 Z. Zhang, Y. Zhao, Q. Gong, Z. Li and J. Li, *Chem. Commun.*, 2013, **49**, 653–661.
10 P. Nugent, Y. Belmabkhout, S. D. Burd, A. J. Cairns, R. Luebke, K. Forrest, T. Pham, S. Ma, B. Space, L. Wojtas, M. Eddaoudi and M. J. Zaworotko, *Nature*, 2013, **495**, 80–84.
11 B. Liu, S. Jie and B. Li, *Prog. Chem.*, 2013, **25**, 36–45.
12 J. Gascon, A. Corma, F. Kapteijn and F. X. Llabres i Xamena, *ACS Catal.*, 2014, **4**, 361–378.
13 J. E. Mondloch, O. K. Farha and J. T. Hupp, *RSC Catal. Ser.*, 2013, **12**, 289–309.
14 H. R. Moon, D.-W. Lim and M. P. Suh, *Chem. Soc. Rev.*, 2013, **42**, 1807–1824.
15 J. Zhuang, C.-H. Kuo, L.-Y. Chou, D.-Y. Liu, E. Weerapana and C.-K. Tsung, *ACS Nano*, 2014, **8**, 2812–2819.
16 M. C. Bernini, D. Fairen-Jimenez, M. Pasinetti, A. J. Ramirez-Pastor and R. Q. Snurr, *J. Mater. Chem. B*, 2014, **2**, 766–774.
17 P. Horcajada, T. Chalati, C. Serre, B. Gillet, C. Sebrie, T. Baati, J. F. Eubank, D. Heurtaux, P. Clayette, C. Kreuz, J.-S. Chang, Y. K. Hwang, V. Marsaud, P.-N. Bories, L. Cynober, S. Gil, G. Ferey, P. Couvreur and R. Gref, *Nat. Mater.*, 2010, **9**, 172–178.
18 Z. Hu, J. D. Benjamin and J. Li, *Chem. Soc. Rev.*, 2014, **43**, 5815–5840.
19 L. E. Kreno, K. Leong, O. K. Farha, M. Allendorf, R. P. Van Duyne and J. T. Hupp, *Chem. Rev.*, 2012, **112**, 1105–1125.
20 G. Lu and J. T. Hupp, *J. Am. Chem. Soc.*, 2010, **132**, 7832–7833.
21 J. C. Rybak, M. Hailmann, P. R. Matthes, A. Zurawski, J. Nitsch, A. Steffen, J. G. Heck, C. Feldmann, S. Goetzendoerfer, J. Meinhardt, G. Sextl, H. Kohlmann, S. J. Sedlmaier, W. Schnick and K. Mueller-Buschbaum, *J. Am. Chem. Soc.*, 2013, **135**, 6896–6902.
22 C.-Y. Sun, X.-L. Wang, X. Zhang, C. Qin, P. Li, Z.-M. Su, D.-X. Zhu, G.-G. Shan, K.-Z. Shao, H. Wu and J. Li, *Nat. Commun.*, 2013, **4**, 2717.
23 P. Horcajada, R. Gref, T. Baati, P. K. Allan, G. Maurin, P. Couvreur, G. Ferey, R. E. Morris and C. Serre, *Chem. Rev.*, 2012, **112**, 1232–1268.
24 J. Wack, R. Siegel, T. Ahnfeldt, N. Stock, L. Mafra and J. Senker, *J. Phys. Chem. C*, 2013, **117**, 19991–20001.
25 A. Calderon-Casado, G. Barandika, B. Bazan, M.-K. Urtiaga and M.-I. Arriortua, *CrystEngComm*, 2013, **15**, 5134–5143.
26 A. Calderon-Casado, G. Barandika, B. Bazan, M.-K. Urtiaga, O. Vallcorba, J. Rius, C. Miravittles and M.-I. Arriortua, *CrystEngComm*, 2011, **13**, 6831–6838.
27 A. Calderon-Casado, G. Barandika, B. Bazan, M.-K. Urtiaga and M.-I. Arriortua, *CrystEngComm*, 2010, **12**, 1784–1789.
28 A. Calderon-Casado, G. Barandika, B. Bazan, M.-K. Urtiaga and M.-I. Arriortua, *PCT Int. Appl.*, WO 2013057350 A1 20130425, 2013.
29 Z.-G. Li, G.-H. Wang, H.-Q. Jia, N.-H. Hu, J.-W. Xu and S. R. Batten, *CrystEngComm*, 2008, **10**, 983–985.
30 L.-L. Wen, D.-B. Dang, C.-Y. Duan, Y.-Z. Li, Z.-F. Tian and Q.-J. Meng, *Inorg. Chem.*, 2005, **44**, 7161–7170.
31 A. J. Blake, N. R. Brooks, N. R. Champness, M. Crew, L. R. Hanton, P. Hubberstey, S. Parsons and M. Schroder, *J. Chem. Soc., Dalton Trans.*, 1999, 2813–2817.
32 Z. He, Z.-M. Wang and C.-H. Yan, *CrystEngComm*, 2005, **7**, 143–150.
33 W. Zheng, X. Liu, J. Guo, L. Wu and D. Liao, *Inorg. Chim. Acta*, 2004, **357**, 1571–1578.
34 J. Lin, L. Wen, S. Zang, Y. Su, Z. Lu, H. Zhu and Q. Meng, *Inorg. Chem. Commun.*, 2007, **10**, 74–76.
35 C. M. Rogers, N. H. Murray, R. M. Supkowski and R. L. La Duca, *Inorg. Chim. Acta*, 2013, **407**, 167–174.
36 E. Shyu, M. A. Braverman, R. M. Supkowski and R. L. LaDuca, *Inorg. Chim. Acta*, 2009, **362**, 2283–2292.
37 S. Sengupta, S. Ganguly, A. Goswami, P. K. Sukul and R. Mondal, *CrystEngComm*, 2013, **15**, 8353–8365.
38 D.-C. Wen, S.-X. Liu and J. Ribas, *Inorg. Chem. Commun.*, 2007, **10**, 661–665.
39 M. A. Withersby, A. J. Blake, N. R. Champness, P. A. Cooke, P. Hubberstey and M. Schroder, *New J. Chem.*, 1999, **23**, 573–575.
40 W.-L. Meng, Z.-H. Zhang, Y. Lv, H. Kawaguchi and W.-Y. Sun, *Appl. Organomet. Chem.*, 2006, **20**, 399–403.
41 M. Kondo, M. Shimamura, S. I. Noro, S. Minakoshi, A. Asami, K. Seki and S. Kitagawa, *Chem. Mater.*, 2000, **12**, 1288–1299.
42 M. A. Withersby, A. J. Blake, N. R. Champness, P. A. Cooke, P. Hubberstey, A. L. Realf, S. J. Teat and M. Schroder, *J. Chem. Soc., Dalton Trans.*, 2000, 3261–3268.
43 W. Yinghua, *J. Appl. Crystallogr.*, 1987, **20**, 258–259.
44 A. Altomare, G. Cascarano, C. Giacovazzo and A. Guagliardi, *J. Appl. Crystallogr.*, 1993, **26**, 343–350.
45 G. M. Sheldrick, *Acta Crystallogr., Sect. A: Found. Crystallogr.*, 2008, **64**, 112–122.

46 V. A. Blatov, *IUCr CommpComm Newsl*, 2006, vol. 7, pp. 4–38, http://www.topos.ssu.samara.ru.
47 H. Zabrodsky, S. Peleg and D. Avnir, *J. Am. Chem. Soc.*, 1992, **114**, 7843–7851.
48 M. Pinsky and D. Avnir, *Inorg. Chem.*, 1998, **37**, 5575–5582.
49 D. C. M. Llunel, J. Cirera, J. M. Bofill, P. Alemany, S. Álvarez, M. Pinsky and D. Yanutir, *SHAPE v1.1a*, 2003.
50 S. Álvarez, P. Alemany, D. Casanova, J. Cirera, M. Llunell and D. Avnir, *Coord. Chem. Rev.*, 2005, **249**, 1693–1708.
51 *Powder Diffraction File - Inorganic and Organic*, ICCD, Pennsylvania, ref. code: 01-080-1268, 2001.
52 O. Khan, *Molecular Magnetism*, VCH Publishers, Weinheim, 1993.
53 J. C. Booner and M. E. Fisher, *Phys. Rev.*, 1964, **135**, A640–A658.